JMEPEG (2006) 15:758-764
DOI: 10.1361/105994906X150902

1059-9495/$19.00

Microstructure and Corrosion Behavior of Shielded Metal Arc-Welded Dissimilar Joints Comprising Duplex Stainless Steel and Low Alloy Steel

P. Bala Srinivasan, V. Muthupandi, W. Dietzel, and V. Sivan

(Submitted October 24, 2003; in revised form August 15, 2004)

This work describes the results of an investigation on a dissimilar weld joint comprising a boiler-grade low alloy steel and duplex stainless steel (DSS). Welds produced by shielded metal arc-welding with two different electrodes (an austenitic and a duplex grade) were examined for their microstructural features and properties. The welds were found to have overmatching mechanical properties. Although the general corrosion resistance of the weld metals was good, their pitting resistance was found to be inferior when compared with the DSS base material.

Keywords corrosion resistance, dissimilar metal welds, hardness, microstructure

1. Introduction

Joining of materials by fusion welding processes is inevitable for engineering applications, although under many circumstances these joints are vulnerable to environmental degradation. It then becomes mandatory to design welds to meet the service requirements with appropriate control over the process conditions, by taking care of chemistry and resultant microstructure. Joining of duplex stainless steel (DSS) to plain carbon steels by gas tungsten arc welding and their microstructural features have been addressed by Barnhouse et al. (Ref 1), but there is not much published information available on this combination of weldments (Ref 2, 3). Although the corrosion behavior of weldments of similar materials has been investigated by a few researchers (Ref 4-6), the information on the properties of the dissimilar weldments, especially those comprising DSS, is very scarce. The current work describes the microstructural features and electrochemical behavior of dissimilar weld joints between a boiler-grade low alloy steel (LAS) and duplex stainless steel (DSS), produced by shielded metal arc welding (SMAW) using two different stainless steel electrodes.

2. Experimental Procedures

The materials used in the current investigation are a boiler-grade LAS and UNS 31,803-grade duplex stainless steel, the chemical compositions of which are given in Table 1. Welds were produced by SMAW, using a nickel-fortified DSS electrode (E2209) and an E309 electrode. For ease of referencing and discussion purposes, the weldments/weld metals produced with E2209 and E309 electrodes shall hereinafter be referred to as "A" and "B", respectively.

Plates, 200 × 80 × 5 mm, were used for producing the joints and a 70° single "V" edge preparation was followed with a root face and root gap of 2 mm each. The welds were produced in four passes (including the one laid after back-gouging the root) using the following parameters: 110-120 A; 22-24 V; and 120-150 mm/min welding speed.

Microstructural features of the different regions of this dissimilar weldment were characterized by conventional metallographic practices, using appropriate etchants for the respective regions, as given in Table 2. Metallographic examination was performed using a high-resolution microscope, and representative regions were photomicrographed. Transverse tensile tests were performed with a horizontal bench-type tensometer to ascertain the strength of weldment and also to identify the region of failure. The tensile samples were prepared in such a way that the entire weldment region (weld metal, heat-affected zones [either side], and base materials) was in the gauge section; a schematic diagram for this configuration is shown in Fig. 1. A hardness traverse (survey) was made across the weldment using a Vickers hardness tester under a 2 N load.

Potentiodynamic polarization studies were performed to assess the corrosion behavior of the weldments, and the tests were conducted in non-deaerated 1 M sodium chloride solution in the as-prepared condition. A three-electrode cell was used for the polarization studies, wherein the sample, saturated calomel, and platinum were used as working, reference, and auxiliary electrodes, respectively. All the tests were performed at a scan rate of 1 mV/s. For each test condition, three experiments were made to ensure the reproducibility/repeatability of results.

3. Results and Discussion

3.1 Microstructural Features

Microstructural features of the DSS and LAS parent materials are shown in Fig. 2(a) and (b), respectively. A dual-phase

P. Bala Srinivasan, V. Muthupandi, and **V. Sivan,** Department of Metallurgical Engineering, National Institute of Technology, Tiruchirappalli 620 015, India; and **P. Bala Srinivasan** and **W. Dietzel,** GKSS-Forschungszentrum, Geesthacht GmbH, Institute for Materials Research, D-21502 Geesthacht, Germany. Contact e-mail: pbs@nitt.edu.

Table 1 Chemical composition of base materials and weld metal (wt.%)

Element	C	S	P	Si	Mn	Cr	Ni	Mo	N	Fe
DSS base material	0.02	0.02	0.03	0.60	1.40	22.20	5.90	2.90	0.15	Balance
Low alloy steel	0.12	0.035	0.03	0.45	0.55	2.10	…	1.05	…	Balance
Weld metal A(a)	0.03	0.02	0.025	0.50	1.70	21.60	7.80	2.95	0.10	Balance
Weld metal B(b)	0.06	0.03	0.03	0.50	1.20	22.30	9.20	0.10	…	Balance

(a) Weld metal A produced with E2209 electrode. (b) Weld metal B produced with E309 electrode

Table 2 Etchants and etching procedure

Material/region	Etchant and etching procedure
LAS-BM and HAZ	2% Nital Temperature 35 °C Swab; duration 45 s
DSS-BM and HAZ	Hydrochloric acid 20 mL Sodium metabisulfite 1 g Distilled water 100 mL Temperature 35 °C Immersion; duration 30-45 s
Weld metal	10% (w/o) oxalic acid solution Electrolytic, 6-9 V Temperature 35 °C Duration 45 s-60 s

structure with near-equal amounts of austenite-ferrite stringers is seen in Fig. 2(a), which characterized the features of the rolled product. A typical grain structure of fine and equiaxed of pro-eutectoid ferrite, with small amounts of globular bainite, was observed in the LAS.

It is well known that, during welding, heat-affected zones are developed on either side of the weld metal adjoining the fusion boundaries due to heat dissipation into the base materials. Figures 3(a) and (b) show the microstructural features of the LAS-weld metal (WM) interface and the associated heat-affected zone close to the fusion boundary, respectively. It is evident from Fig. 3(a) that in the LAS, close to the fusion boundary, a carbon-depleted zone has developed as a result of welding. This is not surprising, and in fact could be expected, as the carbon content in the LAS is slightly higher (0.12% by weight) than that in the weld metal. Hence, the concentration gradient and the congenial thermal cycles experienced during welding would have led to the diffusion of carbon from the LAS side into the weld metal, developing the decarburized region close to the fusion boundary. In addition, the weld metal, being richer in chromium, would have assisted/aided in the migration of carbon from LAS during welding owing to the higher affinity for carbon. The carbon migration from the carbon steel to the high alloy steels/stainless steels during welding has been documented in literature (Ref 7-10).

Figure 4 shows the microstructural features of the LAS-WM interface (weldment A), which is characteristic of fusion welds between materials with different crystal structures (Ref 11). A type II boundary has been observed in the weld metal, just adjacent to the LAS-WM fusion boundary. The occurrence of type II boundaries is reported to be due to the transition in primary solidification behavior caused by the compositional gradient normal to the fusion boundary. In a recent work, it has been shown that formation of this type of boundary is feasible only under conditions of the existence of a ferrite-austenite phase boundary at elevated temperatures (Ref 12).

Despite the fact that the zone between the fusion boundary (LAS side) and the type II boundary looks featureless, the EDS line scan (Fig. 5a) revealed a concentration gradient of alloying elements across this interface. On the other hand, the EDS profile taken across the WM-DSS interface did not show much variation in chemical composition (Fig. 5b). Although there were definite differences in the nickel content in the DSS base material and the bulk weld metal, it was not reflected distinctly in this narrow region, possibly due to the dilution effects close to the interface. An EDS line scan was performed for the weldment "B," and a similar trend as that for the weldment "A" was observed. It would have been much better had electron probe microanalysis been used to quantitatively assess the alloying elements, including carbon and nitrogen, in these regions. Because such an apparatus was not available, assessment of interstitial elements could not be made in this work.

The microstructures of the two weld metals produced using E2209 and E309 electrodes are shown in Fig. 6(a) and (b), respectively. Both welds were composed of austenite and ferrite as microconstituents, but with different morphological features. Weld metal "A" has shown a feature characteristic of a duplex stainless steel weld metal structure, whereas the weld metal "B" has a microstructure similar to those observed in austenitic stainless steel weld joints. It is evident from the above observations that the heat input/dilution during welding and the chemistry of respective welds have a synergistic effect on the phase balance, and thus, has resulted in such contrasting microstructural features.

3.2 Mechanical Properties

Microhardness measurements made at the LAS-WM interface for the weldments A and B are presented in Fig. 7(a). In both the weldments, a dip in hardness was noticed close to the fusion boundary in the LAS side, which is due to the depletion of carbon in this region. A higher hardness was recorded, on either side, just adjoining this carbon-denuded zone in the weldment. In the LAS side, the increase in hardness is due to the tempered martensitic structure that developed during welding, the microstructural features of which are seen in Fig. 3(b). The maximum hardness (266 $HV_{0.2}$) developed in the heat-affected zone of the LAS is acceptable as per codes for structural and power piping applications.

In weldment A, a maximum hardness of ~310 $HV_{0.2}$ was recorded in the zone between the fusion boundary and the type II boundary, whereas in weldment B, a hardness of 295 $HV_{0.2}$ was obtained. To give a better picture of the hardness close to these boundaries, the region marked (encapsulated in ellipse) in

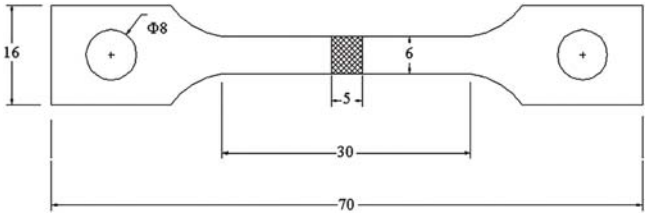

Fig. 1 Schematic diagram of the transverse tensile test specimen

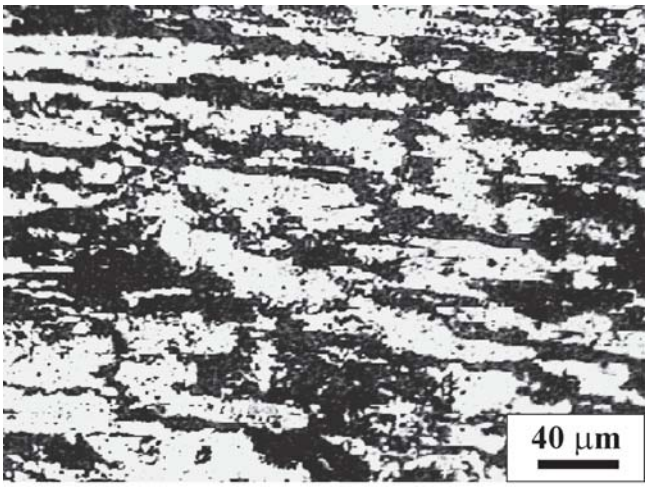

(a)

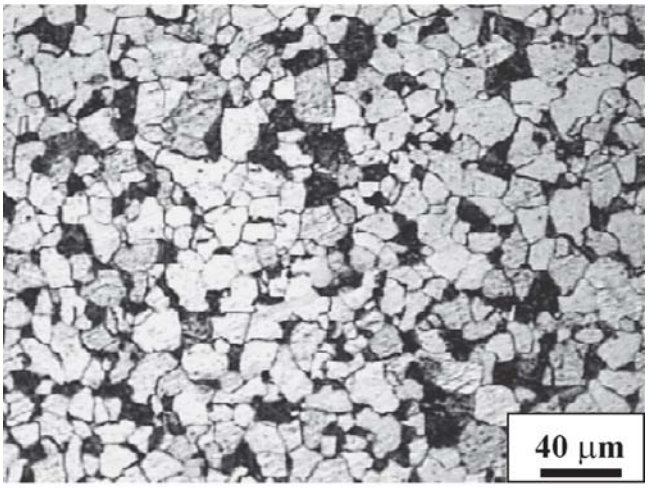

(b)

Fig. 2 Optical micrograph of base materials: (a) DSS; (b) LAS

Fig. 7(a) is expanded to give a better insight of variations and presented as Fig. 7(b). As is seen in Fig. 7, the hardness level in the weld metal was higher in the region close to the fusion boundary, dropping gradually to lower values, and finally matching that of the bulk weld metal ~100 μm from the fusion boundary. The higher hardness in this narrow zone between the two boundaries is attributed to the diffusion of carbon from the relatively higher carbon-containing LAS, leading to formation of martensite and carbides (Ref 1, 13). The hardness of weld metal A was found to be ~270 $HV_{0.2}$ compared with 220 $HV_{0.2}$ for weld metal B, and it is more likely that the variations observed above are due to the differences in chemistry of the respective weld metals.

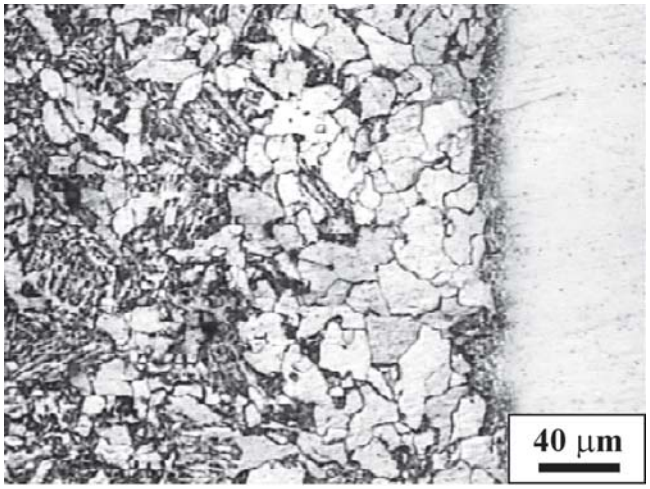

(a)

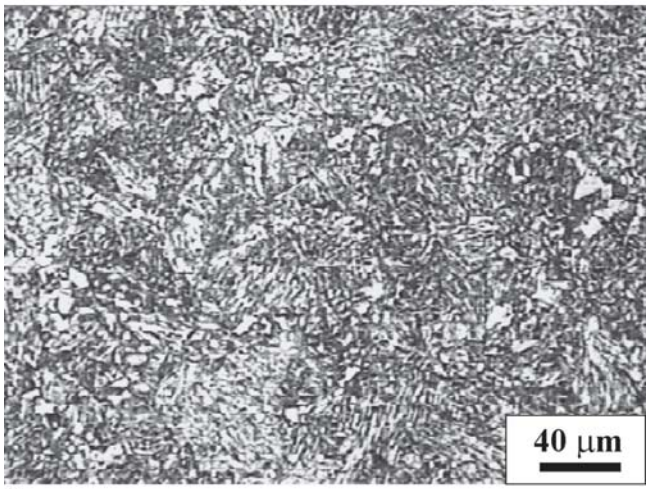

(b)

Fig. 3 (a) Microstructural features of the LAS-weld metal interface; arrow indicates the carbon-denuded zone (near complete ferritic structure); (b) optical micrograph showing the features of the hard zone in the LAS HAZ

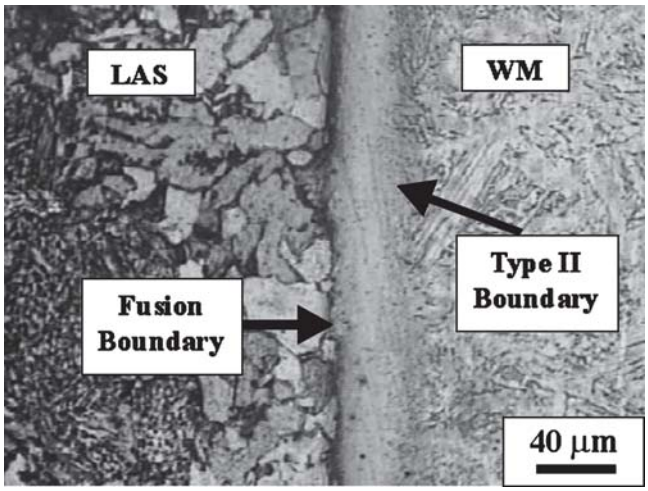

Fig. 4 Microstructure of the LAS-WM interface (electrolytically etched)

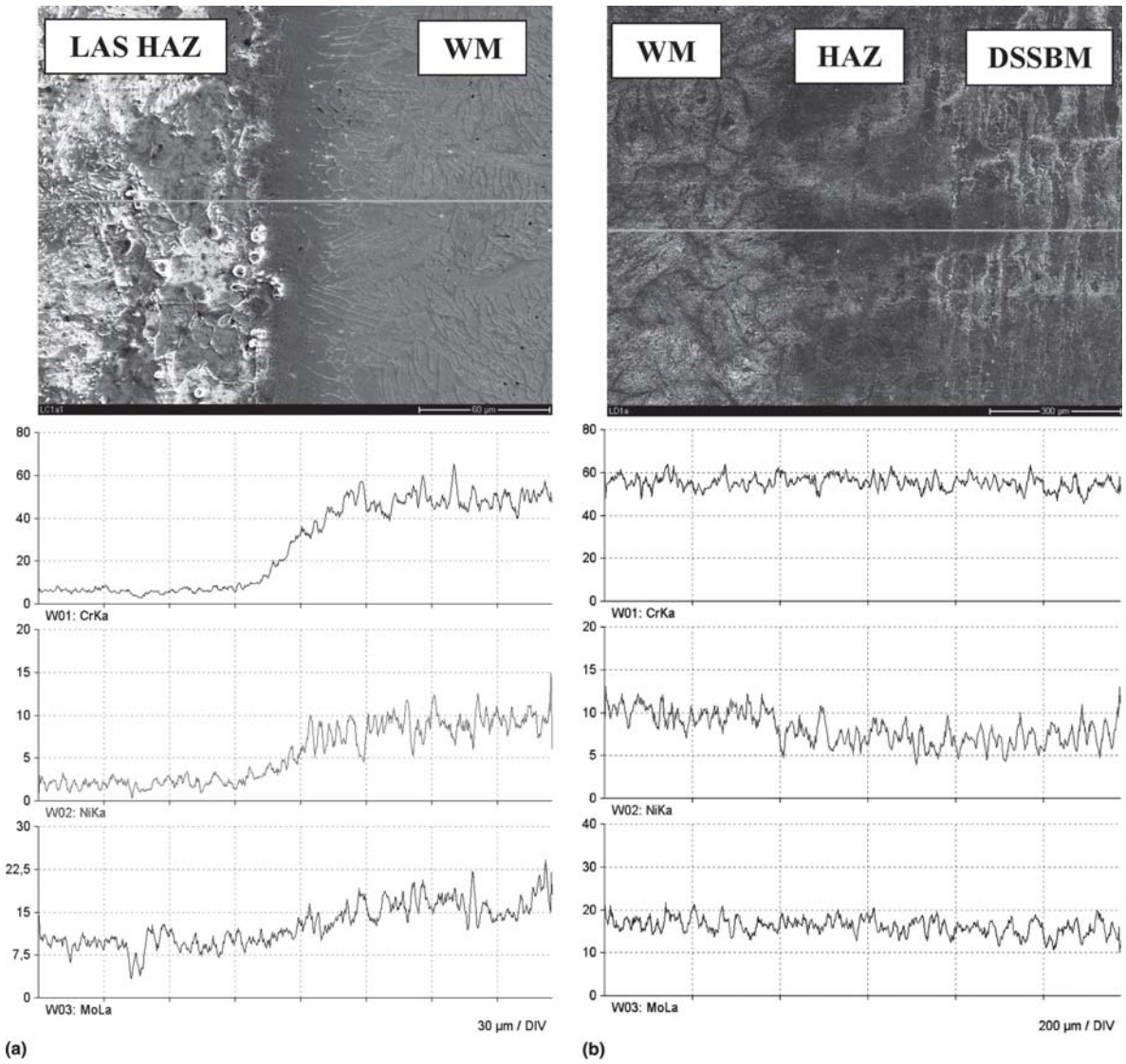

Fig. 5 EDS line scan showing variation of alloying elements across the interface: (a) LAS-WM interface; (b) DSS-WM interface

On the other hand, the heat-affected zone in the DSS side (weld A) was seen to be confined to a very narrow region (~200 μm), which is attributable to the physical metallurgical characteristics of the stainless steel (Ref 14). The heat-affected zone in DSS has a predominantly coarse-grained ferritic structure, with austenite "garlanding" the grain boundaries (Fig. 8). Development of microstructures with such morphological features in the HAZ of DSS weldments has been observed in an earlier investigation (Ref 15). However, there is not much variation in the hardness of the heat-affected zone, with the hardness values being ~265 $HV_{0.2}$. Similar microstructural features and hardness values have also been observed in the HAZ of weldment B.

In the transverse tensile tests, both weldments A and B failed in the LAS base material. It is interesting to note that the development of the soft zone close to the fusion boundary (in the LAS side) did not really influence the tensile behavior, and fracture occurred only in the LAS base material. A macrograph of the tested sample clearly reveals the region and mode of fracture (Fig. 9a), and the associated fractograph (Fig. 9b) shows a predominantly dimpled structure, characteristic of ductile fracture. The above observations highlight that dissimilar weldments have over-matching mechanical properties, which is very much desirable from point of view of weldment design.

3.3 Corrosion Behavior

The potentiodynamic polarization behavior of the LAS base material and the heat-affected zone are depicted in Fig. 10. As can be seen from the plot, the LAS base material has a corrosion potential of −647 mV versus saturated calomel electrode (SCE) compared with −602 mV versus SCE for the heat-affected zone, suggesting that the HAZ of LAS is more noble than its base material counterpart. The LAS base material and HAZ have registered corrosion current density values of 12.9 and 14.5 $\mu A/cm^2$, respectively. Similar observations on the corrosion behavior of the heat-affected zone have been reported in literature (Ref 16, 17). It was observed that a composite structure composed of low-temperature transformation microconstituents, like bainite and tempered martensite, led to lower general corrosion resistance.

Because the HAZ in the DSS side was too small, no attempt

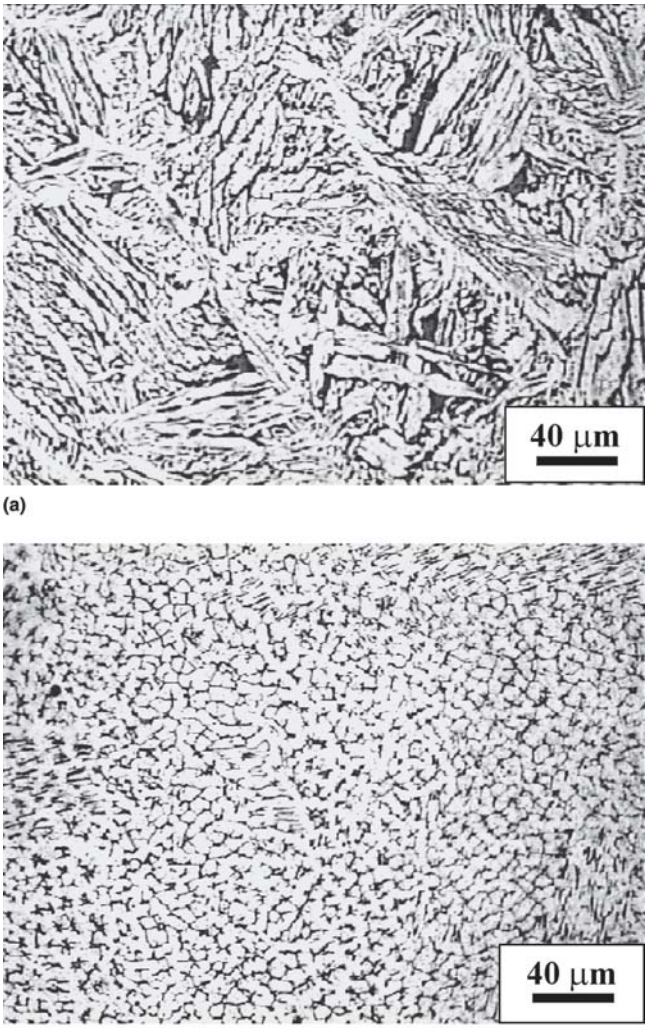

Fig. 6 Optical micrograph showing features of the weld metals: (a) weld metal A; (b) weld metal B

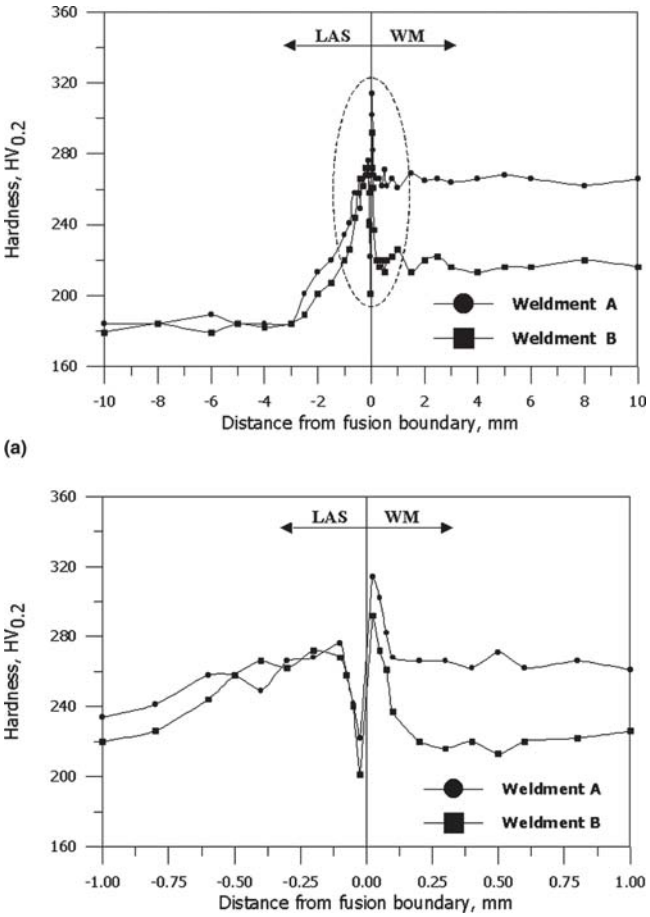

Fig. 7 Microhardness profile across the LAS-WM interface: (a) all regions of weldment (WM-HAZ-BM); (b) expanded view of the section marked in (a) to show the variations close to the boundaries

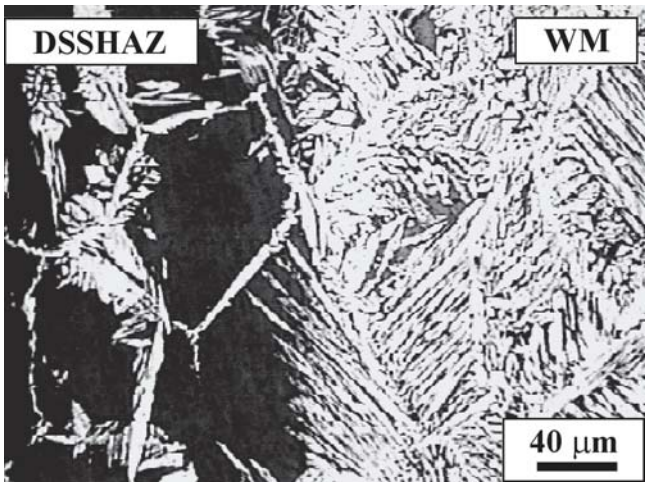

Fig. 8 Microstructure of the DSS HAZ-weld metal interface in weldment A

was made to exclusively assess its corrosion resistance. The corrosion behavior of the DSS base material (DSSBM) and weld metals A and B are depicted in Fig. 11 and the corresponding electrochemical data are presented in Table 3. In the chloride environment, DSSBM has exhibited a corrosion potential of −220 mV versus SCE, which is marginally more noble than the potentials observed for weld metals A and B. Weld metal B, with relatively smaller amounts of ferrite, has registered a lower corrosion current density compared with the DSSBM and weld metal A. In an earlier investigation, it was found that the general corrosion behavior of austenitic stainless steel was better than DSS (Ref 18), and the inferior corrosion resistance of DSS was traced to the galvanic interactions between the austenite and ferrite phases within the matrix. In the current case, the differences in the general corrosion behavior of welds and DSSBM samples could be due to variations observed in the chemistry as well as from morphology, quantity, and/or distribution of microconstituents in the respective samples.

In the potentiodynamic polarization studies in 1 M NaCl solution, weld metal B exhibited better general corrosion resistance than weld metal A and DSSBM. However, weld metal B exhibited a lower pitting corrosion resistance, showing a breakdown at a potential ~442 mV versus SCE. Weld metal A also showed signs of pitting ~730 mV versus SCE, whereas there was no breakdown of passive film in the case of DSSBM. The pitting corrosion behavior of stainless steels is governed by the chemical composition of the alloy, which is primarily due to three important alloying elements: chromium (Cr), molybdenum (Mo), and nitrogen (N). The pitting corrosion resistance

(a)

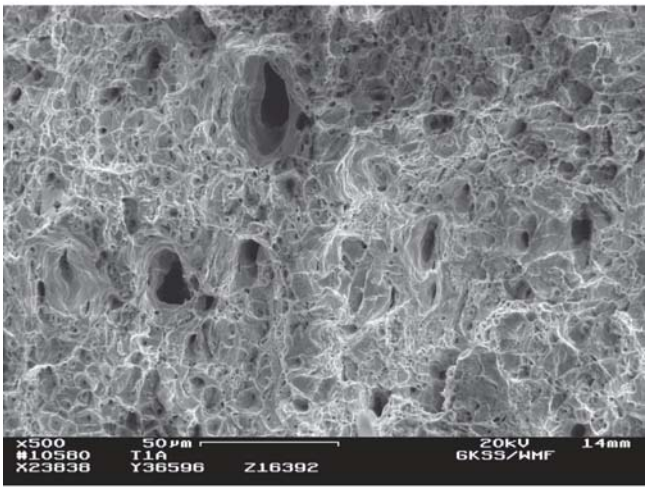

(b)

Fig. 9 (a) Macrograph of the tensile sample (Weldment A) after testing; (b) SEM fractograph of the fracture surface, revealing dimpled structure

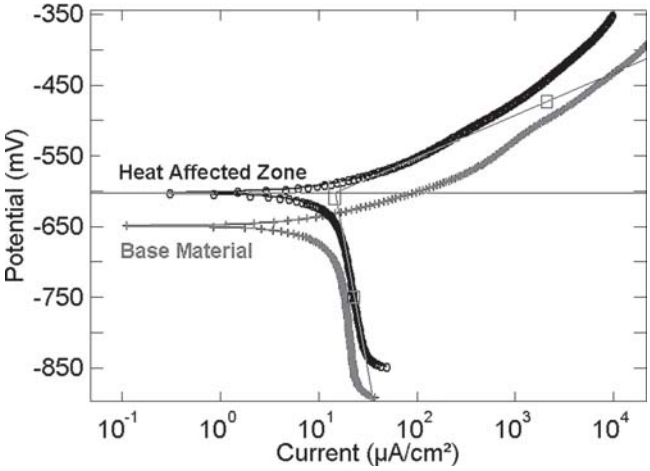

Fig. 10 Potentiodynamic polarization behavior of LAS base material and HAZ in 1 M NaCl solution

of stainless steel weld metals, especially the duplex stainless steels, is generally predicted by calculating the pitting resistance equivalent using the formula given below (Ref 11):

$$\text{Pitting Resistance Equivalent } (PRE)_N = \% \text{ Cr} + 3.3(\% \text{ Mo}) + 16(\% \text{ N})$$

The pitting resistance equivalent values for weld metal A and weld metal B are 33 and 23, respectively, whereas that for the

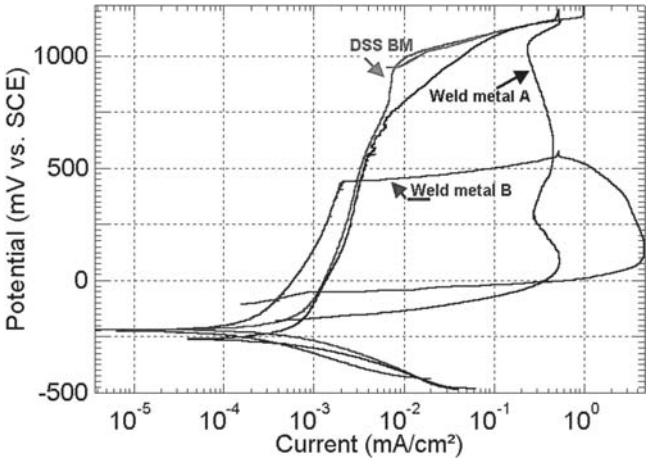

Fig. 11 Potentiodynamic polarization behavior of DSS base material and weld metals A and B in 1 M NaCl solution

DSS base material is 34. Although weld metal A has a PRE_N value much closer to that of the DSSBM, it was found to be susceptible to pitting. It is well known that the presence of nitrogen enhances the pitting resistance of stainless steels (Ref 19-21), and in this case, the lower nitrogen level in the weld metal is the most likely cause for this inferior resistance. On the other hand, for weld metal B, the inferior pitting corrosion resistance can be attributed not only to the absence of nitrogen but also to the very low level of Mo.

It is pertinent to point out that pitting behavior is representative of the bulk section of the respective weld metals. The narrow zone between the fusion boundary and the type II boundary in the LAS side was not included in this assessment. EDS line scans (qualitative) on the weld have revealed a gradient of alloying elements (Cr, Ni, and Mo) across this zone between the two boundaries (Fig. 5a). It is quite probable that this narrow zone in the weld metal, leaner in alloying elements, may very well behave differently in aggressive and hostile environments. The electrochemical behavior of this region still remains to be investigated with the use of advanced electrochemical tools at localized levels, and attempts to assess this are being made.

4. Conclusions

The results of this investigation lead to the following conclusions:

- Joining of DSS to LAS can be done by the SMAW process using either E2209 or E309 electrodes, achieving welds with overmatching strength levels.
- In chloride environments, the LAS HAZ region has a marginally higher corrosion rate than its base material counterpart.
- General corrosion resistance of the weld metal produced with the E309 electrode is better than that produced with the E2209 electrode.
- Both weld metals, produced with E2209 and E309, have inferior pitting resistance when compared with the DSS base material, and the pitting resistance ranking is:

DSS base material > Weld metal A > Weld metal B

Table 3 Electrochemical data for the DSS-LAS weldments in 1 M NaCl solution

Region	Corrosion potential, E_{corr} (mV versus SCE)	Corrosion current density, I_{corr} (μA cm^{-2})	Pitting potential, E_{pit} (mV versus SCE)	Protection potential, E_{prot} (mV versus SCE)
LAS BM	−647	12.90	…	…
LAS HAZ	−602	14.50	…	…
DSSBM	−220	0.37	No pitting	No pitting
Weld metal A	−261	0.42	730	−175
Weld metal B	−229	0.14	442	−84

Acknowledgments

One of the authors (P.B.S.) gratefully acknowledges the Department of Science and Technology, India, for financial support under the framework of the Fast-Track Scheme for Young Scientists. The technical support of Dr. R. Song in performing SEM-EDS studies is thankfully acknowledged.

References

1. E.J. Barnhouse and J.C. Lippold, Microstructure/Property Relationships in Dissimilar Welds Between Duplex Stainless Steels and Carbon Steels, *Weld. J.,* 1998, **77**(12), p 477s-487s
2. N.A. McPherson, K. Chi, M.S. McLean, and T.N. Baker, Structure and Properties of Carbon Steel to Duplex Stainless Steel Submerged Arc Welds, *Mater. Sci. Technol.,* 2003, **19**(2), p 219-226
3. R. Rajeev, I. Samajdar, R. Raman, C.S. Harendranath, and G.B. Kale, Origin of Hard and Soft Zone Formation During Cladding of Austenitic/Duplex Stainless Steel on Plain Carbon Steel, *Mater. Sci. Technol.,* 2001, **17**(8), p 1005-1011
4. L.J. Berchmans, S. Muralidharan, N.S. Rengaswamy, S. Natarajan, V. Sivan, and S.V. Iyer, Stress Corrosion Cracking and Hydrogen Embrittlement Susceptibility Studies on Modified 9Cr-1Mo Steel Weldments in Acidic and Neutral Media, *Br. Corros. J.,* 1996, **31**(3), p 223-226
5. T.M. Majid, S.A.R. Sultan, S.D. Mahdi, and S. Jasim, Effect of Microstructure on Corrosion Rate of Underwater Steel Welds, *Corrosion,* 1990, **46**(1), p 37-42
6. T. Hemmingsen, H. Hovdan, P. Sanni, and N.O. Aagotnes, The Influence of Electrolyte Reduction Potential on Weld Corrosion, *Electrochim. Acta,* 2002, **47**(24), p 3949-3955
7. A. Celik and A. Alsaran, Mechanical and Structural Properties of Similar and Dissimilar Steel Joints, *Mater. Charact.,* 1999, **43**(5), p 311-318
8. Y. Yingyou, R. Kaeshiue, R. Haurshiue, and C. Chen, The Study of Carbon Migration in Dissimilar Welding of the Modified 9Cr-1Mo Steel, *J. Mater. Sci. Lett.,* 2001, **20**(15), p 1429-1432
9. A.A. Omar, Effects of Welding Parameters on Hard Zone Formation at Dissimilar Metal Welds, *Weld. J.,* 1998, **77**(2), p 86s-93s
10. C. Pan and Z. Zhang, Morphologies of the Transition Region in Dissimilar Austenitic-Ferritic Welds, *Mater. Charact.,* 1996, **36**(1), p 5-10
11. T.W. Nelson, J.C. Lippold, and M.J. Mills, Nature and Evolution of the Fusion Boundary in Ferritic-Austenitic Dissimilar Weld Metals, Part 1: Nucleation and Growth, *Weld. J.,* 1999, **78**(10), p 329s-337s
12. T.W. Nelson, J.C. Lippold, and M.J. Mills, Investigation of Boundaries and Structures in Dissimilar Metal Welds, *Sci. Technol. Weld. Joining,* 1998, **3**(5), p 249-255
13. D.J. Kotecki, A Martensite Boundary on the WRC-1992 Diagram, *Weld. J.,* 1999, **78**(5), p 180s-192s
14. R. Gunn, *Duplex Stainless Steels: Microstructure, Properties & Applications,* Abington Publishing, 1997, p 110-112
15. V. Muthupandi, P. Balasrinivasan, and S. Sundaresan, Influence of Nitrogen Addition on the Microstructure and Mechanical Properties of Duplex Stainless Steel Weld Metals, *Steel Res.,* 2002, **73**(9), p 409-413
16. V.S. Voruganti, H.B. Luft, D. Degeer, and S.A. Bradford, Scanning Reference Electrode Technique for the Investigation of Preferential Corrosion of Weldments in Offshore Applications, *Corrosion,* 1991, **47**(5), p 343-351
17. H.H. Huang, W.T. Tsai, and J.T. Lee, The Influences of Microstructure and Composition on the Electrochemical Behaviour of A516 Steel Weldment, *Corros. Sci.,* 1994, **36**(6), p 1027-1038
18. S. Sathiyanarayanan, C. Marikkannu, P. Balasrinivasan, and V. Muthupandi, Corrosion Behaviour of Ti6Al4V and Duplex Stainless Steel (UNS31803) in Synthetic Bio-Fluids, *Anti-Corros. Methods Mater.,* 2002, **49**(1), p 33-37
19. U.K. Mudali, S. Ningshen, A.K. Tyagi, and R.K. Dayal, Influence of Metallurgical and Chemical Variables on the Fitting Corrosion Behaviour of Nitrogen-Bearing Austenitic Stainless Steels, *Mater. Sci. Forum,* 1999, **318-320,** p 495-501
20. H. Matsunaga, Y.S. Sato, H. Kokawa, and T. Kuwana, Effect of Nitrogen on Corrosion of Duplex Stainless Steel Weld Metal, *Sci. Technol. Weld. Joining,* 1998, **3**(5), p 225-232
21. R.B. Bhatt, H.S. Kamat, S.K. Ghosal, and P.K. De, Influence of Nitrogen in the Shielding Gas on Corrosion Resistance of Duplex Stainless Steel Welds, *J. Mater. Eng. Perform.,* 1999, **8**(5), p 591-597